ON THE ROLE OF THERMOELECTRIC HEAT TRANSFER IN THE DESIGN OF SMA ACTUATORS: THEORETICAL MODELING AND EXPERIMENT

By
A. Bhattacharyya, D. C. Lagoudas, Y. Wang and V.K. Kinra
Center for the Mechanics of Composites
Aerospace Engineering Department
Texas A & M University
College Station, TX 77843-3141

ABSTRACT

A combined theoretical/experimental study of the heat transfer in thermoelectric Shape Memory Alloy (SMA) actuators is undertaken in this paper. A one-dimensional model of a thermoelectric unit cell with a SMA junction is developed first and the transient temperatures in the SMA are evaluated for different applied electric current densities. As a first step towards the design of an actuator, a thermoelectric module is assembled in the laboratory for cooling/heating the SMA. Transient temperature profiles are recorded for the monotonic heating and cooling runs for two different materials – copper and SMA (with or without the phase transformation). These recorded profiles are then compared with the predictions from the model; the agreement is reasonable, particularly during the cooling process. Temperature profiles are also recorded for cyclic cooling and heating of copper at a frequency of 0.5 Hz and a good comparison is obtained. Theoretical predictions for thermal cycling of SMA show that it is possible to achieve a frequency of 2 Hz on full phase transformation and 17 Hz on partial transformation of 25%.

1. INTRODUCTION

A major impediment in the operation of dynamic structures is undesirable vibrations. In order to control these vibrations, different high frequency low strain actuators using piezoelectrics have been proposed [Takagi, 1990, Wada *et al.*, 1990] . Recently, a new class of large strain actuators is being studied which utilizes the unique solid-solid phase transformation of Shape Memory Alloys (SMA). These alloys undergo a change in crystal structure from a parent cubic austenitic (A) phase to a number of martensitic (M) variants either upon cooling, or with application of stress [Tanaka, 1986]. The reverse phase change occurs, albeit with some hysteresis, on increasing the temperature and/or removal of stress. These phase changes, triggered by thermomechanical loading, are accompanied by significant deformations and when suitably constrained, large actuation forces (about 3 orders of magnitude higher as compared to piezoelectrics) are generated. This effect is most significant in the Nitinol (Ni-Ti) SMA. The Ni-Ti alloy, or Nitinol, is composed of 50 at.wt. % each of Ni and Ti (or 55% and 45 % by weight of Ni and Ti respectively).

The phase change in a Ni-Ti SMA is accompanied by a significant exchange of heat with the surroundings. The transition is intrinsically rate-independent. Therefore, the time rate of

phase transformation is controlled solely by the time rate of heat transfer. Current heat exchange mechanisms include resistive heating (to trigger the M $\rightarrow$ A phase change) and cooling with forced convection (to trigger the A $\rightarrow$ M phase change). These are not very efficient [Bo and Lagoudas, 1994] and hence any SMA actuator depending on these heat-exchange mechanisms will have a low frequency response, even though the force of actuation may be quite substantial. A novel approach to increase the frequency was proposed by Lagoudas and Kinra (1993). Since thermoelectric heat transfer occurs at the junctions of thermoelectric elements due to the flow of electrical charge carriers, they suggested that the SMA actuator be used directly as one of the junctions of the thermoelectric element. This is expected to make the heat transfer process from the SMA more efficient and consequently increase the frequency of actuation. The thermoelectric heat transfer problem in the context of such an approach is investigated here.

Semiconductors have been used for localized cooling, employing the thermoelectric *Peltier effect*. Depending on the direction of the current, the Peltier effect can be used as a heat sink (refrigeration) or as a heat source (heating) [Domenciali, 1954]. Solid state semiconductors have, in fact, been in use as refrigerators for a long time and thus it was their steady state cooling capability that was of primary interest. Extensive research has been conducted in that area; a comprehensive discussion of thermoelectricity and a summary of steady state response of thermoelectric cooling elements is available [Harman and Honig, 1967]. Interest in the transient response – which controls the actuator frequency – is of more recent origin. Thrasher *et al.* (1992), among others, have addressed this problem, but a concerted analytical effort seems to be missing. The work, herein, seeks to address systematically the issues that arise in the study of the transient thermoelectric response during a heat exchange process from or to the SMA junction using semiconductors.

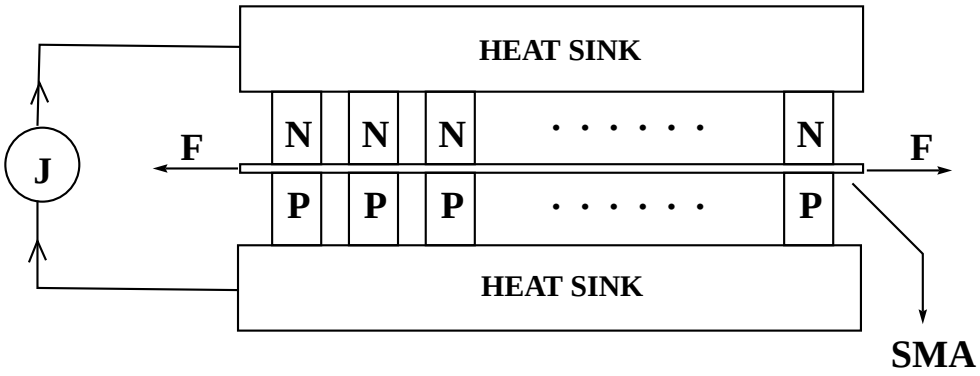

Figure 1: A Proposed SMA actuator

A schematic depiction of a proposed thermoelectrically cooled SMA actuator is given in Fig.1. A thin plate of SMA is sandwiched between pairs of negative doped (N) and positive doped (P) semiconductor elements. Two heat sinks are positioned as shown and the entire assembly is connected to a current source. Each pair of N and P are electrically connected in parallel. When the current is directed from the N to the P element, the Peltier effect causes a reduction in the temperature of the SMA; the converse occurs when the direction of current is reversed. With a change in temperature of the SMA, the desired phase change can be triggered, and if this SMA plate is mechanically constrained at the sides, it produces an actuation force (indicated symbolically as F). For simplicity, we analyse the response of a unit cell comprising a single pair of N and

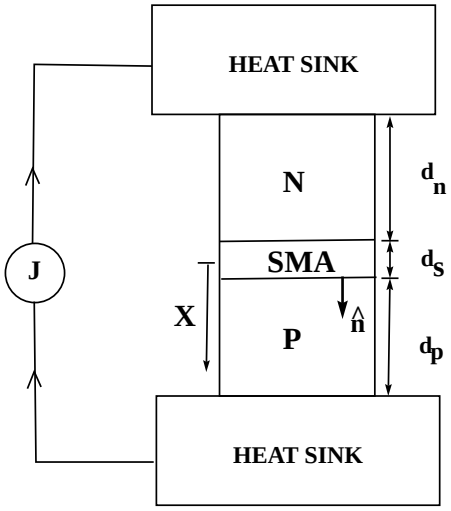

Figure 2: The Unit Cell

P elements. Such a unit cell is depicted in Fig.2. In this paper we will consider the thermoelectric transient response of this unit cell subjected to different electric current densities. The mechanical response is currently under investigation and will be reported in a future communication. Section 2 of the paper provides a one-dimensional (1-D) idealization of the thermal problem in the unit cell. Section 3 presents the nondimensionalised solution, while section 4 includes a parametric study of the solution. Section 5 discusses the experimental setup and concludes with a comparison between the experiment and theoretical predictions.

2. THERMOELECTRIC RESPONSE OF A UNIT CELL

2.1 The Physical Model and its 1-D Formulation

The entire assembly of N/SMA/P elements is flanked by two heat sinks, collectively represented by the unit cell in Fig.2. It is assumed that all the interfaces are in a perfect thermal and electrical contact. The sides of the three phases (N, SMA and P) are exposed to the environment and are prone to convective heat transfer with the surrounding air. An electrical circuit is completed by connecting the cell to a current source. In general, the thermal problem will be three-dimensional. However, if the convective heat transfer is minimal it is reasonable to assume that the temperature varies only along the x-axis, chosen as shown in Fig.2. This allows us to treat this problem as a one-dimensional (1-D) thermoelectric problem. Before we turn to it, it is desirable to briefly discuss the thermoelectric effect. For a rigorous review of the theory, the interested reader is referred to Domenciali (1954).

The flow of electrons (or holes) in semiconductors of the N (or the P) type results in a flow of electrical current. If two dissimilar semiconductors are in contact to form a closed circuit and a temperature differential is maintained between the two junctions, an electric current will flow. This is the well-known Seebeck effect [Domenciali, 1954], based on which thermocouples operate. Conversely, if the circuit is closed by connecting it to a current source and assuming that there is no temperature differential to begin with, the flow of current will create a temperature differential between the junctions where the dissimilar metals meet. This is the Peltier effect, which we propose to use for the thermal cycling of the SMA. As will be seen subsequently, this effect manifests itself through the discontinuity of the heat flux at the interface of the SMA with the N and P

thermoelectric elements. In the sequel, an arrow over a letter will denote a vector quantity and those with a hat will denote unit vectors, unless otherwise mentioned. The inner product of two vectors, $\vec{A}$ and $\vec{B}$, is symbolically written as $\vec{A}.\vec{B}$.

We denote the heat flux vector in the ith phase as $\vec{Q}_i$ and define a unit normal, $\hat{n}$, in the positive x direction (as shown in Fig.2). Recalling that the temperature variation is taken along the x-axis only, we have $\vec{Q}_i = -k_i \frac{\partial T_i}{\partial x}\hat{n}$. The governing equation for the 1-D heat conduction problem then is

$$k_i \frac{\partial^2 T_i(x,t)}{\partial x^2} + \rho_i J^2 - h_i \frac{P}{A}[T_i(x,t) - T_0] = C_i \frac{\partial T_i(x,t)}{\partial t} \ , \quad (i = N, S, P) \ , \tag{1}$$

where the convective heat transfer occuring along the sides of the respective phases has been approximately included as a source term. For brevity, the SMA is denoted as phase S. The thermal conductivity of the ith phase is k_i, $T_i(x,t)$ is the temperature at the location x at time t and ρ_i is the electrical resistivity of the ith phase. The magnitude of the current density is J and h_i is the convection coefficient pertaining to the ith phase. The cross-section of any phase perpendicular to the x-axis is taken to have a perimeter P and area A, respectively. T_0 is the ambient temperature and C_i is the heat capacity per unit volume of the ith phase. All material properties are assumed to be constant, except for C_s for the SMA phase, which is a function of temperature during the phase transformation.

Unlike a conventional heat conduction problem where the assumption of a perfect thermal interface implies continuity of temperature and heat flux, thermoelectric heat transfer manifests itself as a jump discontinuity in the heat flux at the interfaces. When a current J flows from N to SMA or from SMA to P, heat is absorbed at the interface. This is a unique property found only in thermoelectric materials and for the stated current direction, the Peltier effect acts as a heat sink distributed at the interface. We note that the energy absorbed at the interface is proportional to the interface temperature (in absolute units) and the current density and is exactly equal to the difference in heat flux coming out of the SMA, $\vec{Q}_s$, and that conducted into the P, $\vec{Q}_p$. The energy balance at the SMA/P interface then is (Domenciali, 1954)

$$(\vec{Q}_s - \vec{Q}_p).\hat{n} = (\alpha_p - \alpha_s)(\vec{J}.\hat{n}) \ T_P(\frac{1}{2}d_s, t) \ , \tag{2}$$

The parameters α_p and α_s are known as the Seebeck coefficients of the P and the SMA respectively. In fact, the Peltier and Seebeck effects mentioned in the beginning of this section are two different phenomena but are controlled by the same parameter, namely the Seebeck coefficient. A detailed discussion of the latter is beyond the scope of this paper. Since $\alpha_p = 2.15 \times 10^{-4} \ V/K$ (Melcor, 1992) and $\alpha_s = 1.2 \times 10^{-5} \ V/K$ (Jackson *et al.*, 1972), the quantity on the right hand side of Eq.(2) is indeed positive if the current is directed from the SMA to the P. A similar equation for energy balance is now written for the N/SMA interface as

$$(\vec{Q}_s - \vec{Q}_n).\hat{n} = (\alpha_n - \alpha_s)(\vec{J}.\hat{n}) \ T_n(-\frac{1}{2}d_s, t) \ . \tag{3}$$

Since $\alpha_n = -\alpha_p$ (Melcor,1992) and $\vec{J}.\hat{n} > 0$, the quantity on the right hand side of Eq.(3) is negative. Once again, heat is absorbed at the interface. It is now apparent that when N and P elements are used in pairs and the current is directed from the N to the P, the Peltier effect acts as a heat sink at both interfaces. On the contrary, if the current direction is reversed, the Peltier effect acts as a heat source resulting in heating of the junction. Commercially, Bismuth Telluride

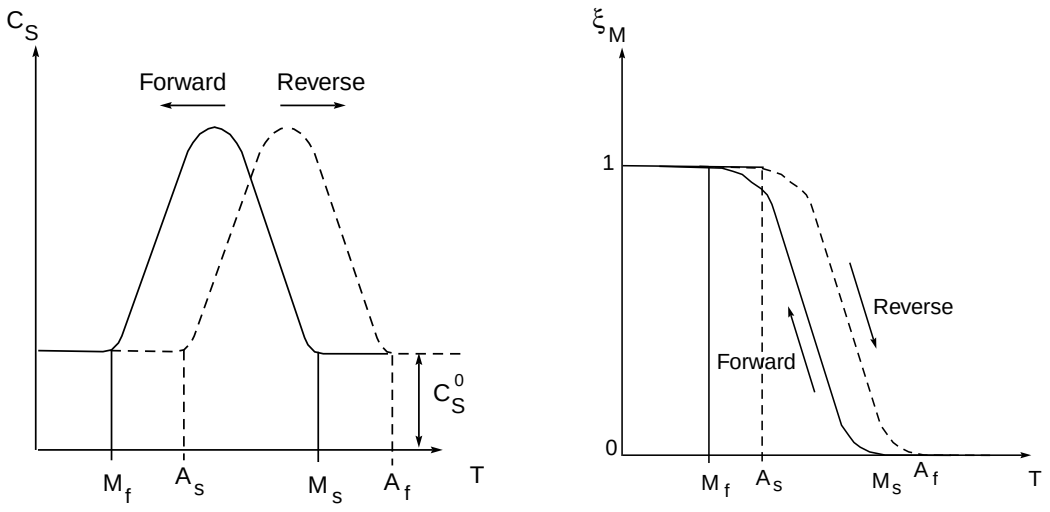

Figure 3: (a) Schematic dependence of C_S on temperature and (b) the evolution of martensite volume fraction, ξ_M, during the forward and reverse transformations.

(Bi-Te) is used in semiconductor applications as it possesses one of the highest magnitudes of α_p (= - α_n) at room temperature. As an aside, we note that most metals/alloys are capable of displaying thermoelectric effects. However, like SMAs, their Peltier effect is very feeble compared to that of a semiconductor; for example, $\alpha_p \approx 18\alpha_s$ for the materials under consideration.

At both interfaces, the temperature is taken to be continuous. Thus

$$T_S(\frac{1}{2}d_S, t) = T_P(\frac{1}{2}d_S, t) \quad , \quad T_S(-\frac{1}{2}d_S, t) = T_N(-\frac{1}{2}d_S, t) \ , \ \text{for all t} \ . \tag{4}$$

The heat sinks are assumed to be at an ambient temperature,T_0, at all time t. Assuming perfect interfaces between the P (or N) and the heat sink, the isothermal boundary conditions become

$$T_P(d_P + \frac{1}{2}d_S, t) \ = \ T_0 \ \text{ and } \ T_N(-d_P - \frac{1}{2}d_S, t) = T_0 \ , \ \text{for all t} \ . \tag{5}$$

The initial conditions of temperature in the ith phase at any x and $t = 0$ is stated as

$$T_i(x, 0) = T_i^{in}(x) \qquad\qquad (i = N, S, P) \ , \tag{6}$$

where $T_i^{in}(x)$ is the initial temperature distribution in the ith phase.

The heat capacity, C_S, of the SMA appearing in Eq.(1) undergoes a significant change during the phase transformation (the heat capacity of the solid state elements are taken to be constant). Before we proceed to solve the heat conduction problem in the context of such a change, we turn to a short discussion of the heat capacity of the SMA.

2.2 The Shape Memory Alloy

As a SMA is cooled, starting to transform from a parent austenitic phase to a product martensitic phase, it undergoes a change in the heat capacity, C_S, during the course of the transformation. A schematic description of this change with the temperature is shown in Fig.3(a), where

the martensitic start temperature is denoted by M_s and the martensitic finish temperature by M_f during cooling. This change is sometimes referred to as the forward transformation. The heat capacities of stable martensite and austenite are slightly different (Jackson *et al.*, 1972); however both are assumed to be equal in order to keep the analysis simple. The symbol C_S^0 represents the heat capacities of both phases.

The latent heat of the forward transformation is defined as $\int_{M_s}^{M_f}(C_S - C_S^0)dT$; it is apparent from Fig.3(a) that the integral will turn out to be a negative quantity indicating the exothermic nature of the transformation. We symbolically represent this latent heat as $-H$ $(H > 0)$. The reverse transformation from martensite to austenite occurs during heating. The austenite start temperature is denoted by A_s and the austenite finish temperature by A_f. The latent heat is defined as $\int_{A_s}^{A_f}(C_s - C_s^0)dT$; this integral is positive indicating the endothermic nature of the transformation. The magnitudes of the latent heat are similar during the forward and the reverse transformations(Jackson,1972 and deBlonk,1995) and will be assumed identical here for simplicity. The latent heat of a typical Ni-Ti SMA has been experimentally determined and reported for the reverse transformation only(refer Fig.65 of Jackson *et al*, 1972). Using their figure, we numerically computed $H = 0.0618\ J/mm^3$. Using this value of H for both transformations, we propose an empirical relation describing the dependence of C_S on T. For the forward transformation, it is

$$C_S = C_S^0 + H\frac{ln(100)}{|M_s - M_f|}e^{-\frac{2ln(100)}{|M_s-M_f|}|T-\frac{M_s+M_f}{2}|} \qquad M_f \leq T \leq M_s\ , \tag{7}$$

and for the reverse transformation, we have

$$C_S = C_S^0 + H\frac{ln(100)}{|A_s - A_f|}e^{-\frac{2ln(100)}{|A_s-A_f|}|T-\frac{A_s+A_f}{2}|} \qquad A_s \leq T \leq A_f\ . \tag{8}$$

For most SMAs, the range $M_f - M_s$ and $A_s - A_f$ are disjoint. We defined the variance,σ, of the error between the curvefit and the experimental data as

$$\sigma = \sqrt{\frac{1}{N}\sum_{i=1}^{N}\left(1 - \frac{C_s(i)}{C_s^{exp}(i)}\right)^2} \times 100\ , \tag{9}$$

where N is the number of total data points available, $C_s^{exp}(i)$ is the experimental measurement of the heat capacity at the ith measurement of temperature and $C_s(i)$ is the corresponding curve-fitted value obtained from Eq.(8) at $A_s = 44.3^0C$ and$A_f = 62.7^0C$ (these values are from Jackson's data). The variance of this error is about 4.35 %. Therefore, the empirical relation of Eq.(8) simulates the experimental data of Jackson quite well. Note that this function has been chosen as it describes the experimental data satisfactorily. It has no other significance.

During the forward (reverse) transformation, the SMA gradually changes with temperature from austenite to martensite (and vice-versa). The changing volume fraction of martensite has been modeled empirically by the exponential model of Tanaka (1986), the cosine model of Liang and Rogers (1990) and very recently by a more fundamental thermodynamic approach of Boyd and Lagoudas (1994). However, for now, we use the exponential model for which the martensitic volume fraction, ξ_M, during the forward transformation is given by

$$\xi_M = 1 - exp\left[\frac{ln(0.01)}{(M_s - M_f)}(M_s - T)\right]\ , \quad M_f \leq T \leq M_s\ , \tag{10}$$

whereas during the reverse transformation it is given by

$$\xi_M = exp\left[\frac{ln(0.01)}{(A_s - A_f)}(A_s - T)\right] \ , \quad A_s \leq T \leq A_f \ . \tag{11}$$

Since there is no explicit dependence of ξ_M on time, the transformation is inherently rate-independent. The evolution of ξ_M will depend on how fast T changes or how rapidly the heat exchange process occurs. The nonlinearity in the heat capacity and the evolving volume fraction of martensite will be needed for the thermal analysis in the last section.

3. THE SYMMETRIC 1-D PROBLEM AND THE SOLUTION

3.1 The Nondimensional Symmetric 1-D Problem

The 1-D problem posed in Eqs.(1)-(6) will be first solved analytically assuming that the heat capacity of all phases *including that of the SMA* is constant. The solution will then be extended numerically in the last section to include the effect of the change in the heat capacity of the SMA during the transformation. We recall that $\alpha_n = -\alpha_p$; all other properties of the N and P semiconductor elements are equal (Melcor, 1992). Recalling that $\alpha_p \approx 18\alpha_s$, it would not be unreasonable to set $\alpha_s \approx 0$. For simplicity, we assume that the length of the N and P elements are identical ($d_N = d_P$) and the initial conditions of Eq.(6) are symmetrical about the origin. In that case, the temperature distribution, in light of the boundary conditions given by Eq.(5) will become symmetric about the origin if the interface conditions of Eqs.(2)-(3) are also symmetric; this will occur if the net heat flow at the SMA/P and SMA/N interfaces are equal in magnitude and opposite in direction. In other words, we have to show that $(\vec{Q}_s - \vec{Q}_p).\vec{n} = -(\vec{Q}_s - \vec{Q}_n).\vec{n}$, where the vector $\vec{Q}_s$ on the left is evaluated at the SMA/P interface and the one on the right at the SMA/N interface. This is easily shown to be the case. Assume that the entire system starts from the ambient temperature T_0 at $t = 0$, when the current is switched on. At that instant, $T_p(\frac{1}{2}d_s, t) = T_n(-\frac{1}{2}d_s, t) = T_0$ in Eqs.(2)-(3). Since $\alpha_s \approx 0$ and $\alpha_n = -\alpha_p$, such a condition is met. Thus at $t = 0$, the thermoelectric problem is symmetrical about the origin. This implies that after every subsequent increment of time (considered as small as we please), the new temperature distribution will also be symmetrical about the origin and by implication will maintain the symmetry in the interface conditions of Eqs.(2)-(3).

While convective heat transfer depends on the fluid (to which convection is occurring) and the geometry of the body (from which convection is taking place), the material of the body is expected to influence the convection only when it is forced. This is because when convection is forced, the heat transfer depends significantly on the boundary layer of the fluid that develops at the fluid-body interface. The thickness of this layer is controlled by the friction at the interface, which in turn depends on the material the body is made of. However, h, is independent of the material makeup for free convection. Since the experiments have been conducted under free-convection conditions, we shall adopt a common h for all three phases (N/SMA/P).

Before the symmetric temperature profile of the constituent phases are given, it is desirable to non-dimensionalize the governing equations (1)-(6) using non-dimensional groups which are obtained by the application of the Buckingham-π theorem (Buckingham, 1914). Unless mentioned otherwise, an English or Greek letter representing a dimensional quantity will have a corresponding non-dimensional counterpart denoted by the same letter with an overbar. These groups are listed

below:

$$\text{Normalized Spatial Co-ordinate: } \bar{x} = \frac{x}{d_p} \ , \qquad \text{Normalized Time: } \bar{t} = t\left(\frac{C_p d_p^2}{k_p}\right)^{-1} \ ,$$

$$\text{Normalized Absolute Temperature: } \bar{T} = \frac{T}{T_0} - 1 \ , \qquad \text{Normalized Current: } \bar{J} = J d_p \sqrt{\frac{\rho_p}{k_p T_0}} \ ,$$

$$\text{Normalized Seebeck coefficient: } \bar{\alpha} = \alpha_p \sqrt{\frac{T_0}{k_p \rho_p}} \ , \qquad \text{Normalized Convection coefficient: } \bar{h} = h \frac{P}{A} \frac{d_p^2}{k_p} \ ,$$

$$\text{Relative Thermal Conductivity of SMA: } \bar{k} = \frac{k_s}{k_p} \ , \qquad \text{Relative Electrical Resistivity of SMA: } \bar{\rho} = \frac{\rho_s}{\rho_p} \ ,$$

$$\text{Relative Heat Capacity of SMA: } \bar{C} = \frac{C_s}{C_p} \ , \qquad \text{Relative Length of SMA: } \bar{d} = \frac{d_s}{2 d_p} \ . \tag{12}$$

Recalling that due to symmetry of the temperature field about $x = 0$, we need only concentrate on the equations pertaining to the SMA/P section of the unit cell ($0 < x < 1 + \bar{d}$). The governing equation (1) for the SMA element then reduces to

$$\bar{k} \frac{\partial^2 \bar{T}_s(\bar{x}, \bar{t})}{\partial \bar{x}^2} + \bar{\rho} \bar{J}^2 - \bar{h} \bar{T}_s(\bar{x}, \bar{t}) = \bar{C} \frac{\partial \bar{T}_s(\bar{x}, \bar{t})}{\partial \bar{t}} \quad (0 < \bar{x} < \bar{d}) \ , \tag{13}$$

whereas for the P it is given by

$$\frac{\partial^2 \bar{T}_p(\bar{x}, \bar{t})}{\partial \bar{x}^2} + \bar{J}^2 - \bar{h} \bar{T}_p(\bar{x}, \bar{t}) = \frac{\partial \bar{T}_p(\bar{x}, \bar{t})}{\partial \bar{t}} \quad (\bar{d} < \bar{x} < 1 + \bar{d}) \ . \tag{14}$$

The normalized conditions of the continuity in temperature and jump discontinuity in the heat flux at the SMA/P interface result in

$$\begin{aligned} \bar{T}_s(\bar{d}, \bar{t}) &= \bar{T}_p(\bar{d}, \bar{t}) \ , \\ -\bar{k} \frac{\partial \bar{T}_s(\bar{d}, \bar{t})}{\partial \bar{x}} &= -\frac{\partial \bar{T}_p(\bar{d}, \bar{t})}{\partial \bar{x}} + \bar{\alpha} \bar{J} (1 + \bar{T}(\bar{d}, \bar{t})) \ , \ \bar{t} > 0 \ . \end{aligned} \tag{15}$$

Due to the symmetry of the temperature field, the heat flux at $\bar{x} = 0$ vanishes for all $\bar{t}$, i.e.

$$\frac{\partial \bar{T}_s(0, \bar{t})}{\partial \bar{x}} = 0 \ , \quad \bar{t} > 0 \ , \tag{16}$$

while at $\bar{x} = 1 + \bar{d}$,

$$\bar{T}_p(1 + \bar{d}, \bar{t}) = 0 \ . \tag{17}$$

The normalized initial conditions are

$$\bar{T}_i(\bar{x}, 0) = \bar{T}_i^{in}(\bar{x}) \qquad (\text{ i =P, S}) \ . \tag{18}$$

3.2 The Solution

The solution of a one-dimensional heat conduction problem for multiple parallel layers with perfect interfaces (with continuity of temperature and heat flux) was given by Tittle (1965) using separation of variables. The solution to our problem represents an extension of their formulation

with the difference that in our case, we have a jump in the heat flux at the interface due to the Peltier effect, as evident from Eq.(15). Briefly, the linearity of the heat equation allows us to decompose the solution for the temperature field into a steady state and a transient part. Then, following Tittle (1965), we solve for the transient component as an infinite series of orthogonal eigenfunctions; these functions are orthogonalized through the use of certain weighting parameters which turn out to be the heat capacities of the individual phases. As it has been derived by decomposing the temperature field, $T(x,t)$, into a steady state part, $T^s(x)$, and a transient part, $T^c(x,t)$, it is convenient to present the solution in terms of their corresponding non-dimensional quantities, $\bar{T}^s(\bar{x}) = T^s(x)/T_0 - 1$ and $\bar{T}^c(\bar{x},\bar{t}) = T^c(x,t)/T_0$. The symmetry of the temperature field about $x = 0$ implies $\bar{T}_i(\bar{x},t) = \bar{T}_i(-\bar{x},t)$. It is then sufficient to give the solution for the nondimensionalized temperature in terms of the absolute value of x, $|x|$.

Temperature Distribution in the SMA $(0 \leq |\bar{x}| \leq \bar{d})$

The non-dimensional temperature, $\bar{T}_s(|\bar{x}|,\bar{t})$, in the SMA is

$$\bar{T}_s(|\bar{x}|,\bar{t}) = \bar{T}_s^s(|\bar{x}|) + \bar{T}_s^c(|\bar{x}|,\bar{t}) \ , \tag{19}$$

where

$$\bar{T}_s^s(|\bar{x}|) = 2C_1 cosh\left(\sqrt{\frac{\bar{h}}{\bar{k}}}|\bar{x}|\right) \ + \ \frac{\bar{\rho}\bar{J}^2}{\bar{h}} \ , \tag{20}$$

and

$$\bar{T}_s^c(|\bar{x}|,\bar{t}) = -e^{-\bar{h}\bar{t}} \sum_{n=1}^{\infty} \frac{B_n sin\beta_{p,n}}{cos\left(\beta_{s,n}\bar{d}\right) cos\left(\beta_{p,n}\left[1+\bar{d}\right]\right)} cos(\beta_{s,n}|\bar{x}|) e^{-\beta_{p,n}^2 \bar{t}} \ . \tag{21}$$

Temperature Distribution in the Semiconductor elements $(\bar{d} \leq |\bar{x}| \leq 1 + \bar{d})$

The non-dimensional temperature, $\bar{T}_p(|\bar{x}|,\bar{t})$, in the P (and N) elements can be written as the sum of its steady-state component, $\bar{T}_p^s(|\bar{x}|)$, and its transient component, $\bar{T}_p^c(|\bar{x}|,\bar{t})$, as

$$\bar{T}_p(|\bar{x}|,\bar{t}) = \bar{T}_p^s(|\bar{x}|) + \bar{T}_p^c(|\bar{x}|,\bar{t}) \ , \tag{22}$$

with

$$\bar{T}_p^s(|\bar{x}|) = C_2\left\{e^{\sqrt{\bar{h}}|\bar{x}|} - e^{\sqrt{\bar{h}}\left(2\left[1+\bar{d}\right]-|\bar{x}|\right)}\right\} + \bar{J}^2\bar{h}^{-1}.\left\{1 - e^{\sqrt{\bar{h}}\left(1+\bar{d}-|\bar{x}|\right)}\right\} \ , \tag{23}$$

and

$$\bar{T}_p^c(|\bar{x}|,\bar{t}) = -e^{-\bar{h}\bar{t}} \sum_{n=1}^{\infty} \frac{B_n}{cos\left(\beta_{p,n}\left[1+\bar{d}\right]\right)} sin\left(\beta_{p,n}\left[|\bar{x}|-1-\bar{d}\right]\right) e^{-\beta_{p,n}^2 \bar{t}} \ . \tag{24}$$

The parameters C_1, C_2 and B_n in Eqs. (20),(21),(23) and (24) have been given in the Appendix.

4. THEORETICAL RESULTS

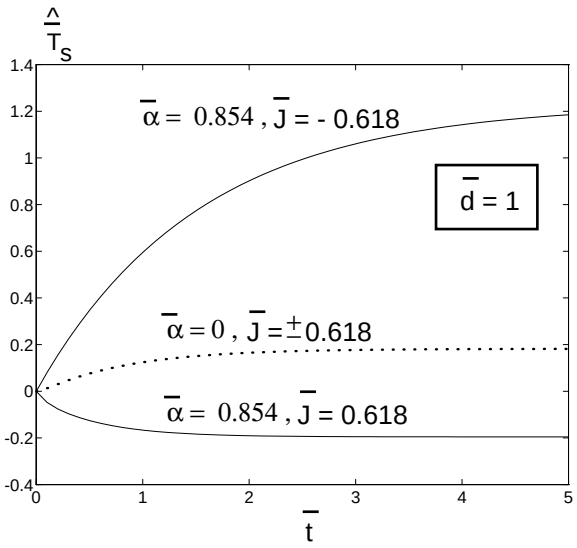

Figure 4: Influence of the directional effect of the current density, $\bar{J}$, on heating and cooling of the SMA.

4.1 Constant C_s (i.e. in absence of phase transformation)

The material parameters of the Ni-Ti SMA from Jackson *et al.* (1972) and that of the N and P semiconductor elements at the room temperature, $T_0 = 296K$, obtained from Melcor (1992), are given in Table 1,

	$\alpha(V/K)$	k $(J/(mm.s-K)$	$\rho(\Omega$-mm)	C $(J/(mm^3-K)$)
SMA	1.2×10^{-5}	2.2×10^{-2}	6.3242×10^{-4}	2.12×10^{-3}
P	2.15×10^{-4}	1.63×10^{-3}	1.15×10^{-2}	4.35×10^{-3}

Table 1. Material Constants of SMA and Semiconductor elements.

where the value of C for SMA is synonymous with the symbol C_s^0 (used in Eqs.(7)-(8)). The magnitude of the latent heat, H, is taken as 0.0618 J/mm^3 (Jackson *et al.*, 1972). The martensitic start and finish temperatures are 23^0 C and 5^0 C respectively whereas the austenitic start and finish temperatures are 29^0C and 51^0 C [Boyd and Lagoudas, 1994]. Incropera and DeWitt (1984) have given a range of values, $5 - 25 \times 10^{-6}$ J/(mm^2.s-K) (from their Table 1-2, pg.16). It can be shown from their analysis that given the current experimental conditions of free convective heat transfer from the N/SMA/P in air, the computed h is approximately $9 \times 10^{-6} J/(mm^2.s-K)$. We shall however choose the highest value in the range, $25 \times 10^{-6} J/(mm^2.s-K)$ to assess parametrically the severity of its effect on the cooling (or heating) due to the Peltier Effect. Using this assumed value of h to embody free convection in air, we compared the results of the model with that for $h = 0$ (no convection). The difference is marginal. Such is also borne out by experiments done in air and in vaccum (no convection). If, however, the model is used to compare with experiments subjected to forced convection in air, it would be more appropriate to use a h pertaining to the geometry of the experimental model and the type of the materials involved (that is, use different h for convection from the surfaces of N,SMA and P respectively). Once the material properties and the geometrical parameters are fixed, six of the ten non-dimensional groups are fixed, namely,

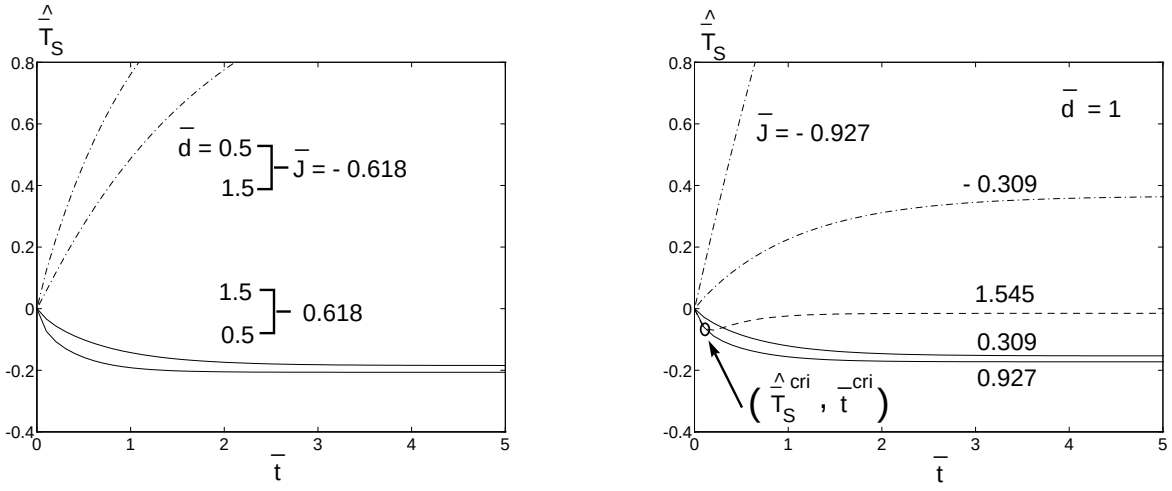

Figure 5: Influence of (a) length, $\bar{d}$, and (b) the current density, $\bar{J}$ on the heating and cooling of the SMA.

$\bar{\alpha}, \bar{h}, \bar{k}, \bar{C}, \bar{\rho}$ and $\bar{d}$ (we take $P/A = 1\ mm^{-1}$ and $T_0 = 296K$). Unless otherwise mentioned, we shall use the non-dimensional quantities henceforth. We begin the analysis by examining the influence of the directional effect of the current on the temperature of the SMA assuming that it does not undergo any phase change (and consequently its heat capacity stays unchanged at C_S^0).

We now introduce a length-averaged nondimensional temperature of the SMA

$$\hat{\bar{T}}_s = \frac{1}{\bar{d}} \int_0^{\bar{d}} \bar{T}_s(|\bar{x}|, \bar{t}) d|\bar{x}|, \tag{25}$$

where the hat over $\bar{T}_s$ indicates the length average (the hat used here is not to be confused with the one used for an unit vector). This average temperature is a function of time; for brevity, however, we write it as $\hat{\bar{T}}_s$ and not $\hat{\bar{T}}_s(t)$. The average temperature will become especially useful in numerically solving the thermoelectric problem when C_s is no longer constant (i.e. during phase transformation); this will be discussed in detail in the next section. For now, we examine the evolution of the average temperature with time, for a constant value of C_s. Such a dependence has been displayed in Fig.4 against the time, $\bar{t}$, at two levels of the current density, $\bar{J}$, both at the same value of the SMA length, $\bar{d} = 1$ and a Seebeck coefficient, $\bar{\alpha} = 0.854$. The lower solid curve corresponds to a positive $\bar{J}$ ($\bar{J}$ is positive when it is directed from the N to the P) and the upper solid curve corresponds to a negative $\bar{J}$. In the former case, the Peltier effect acts as a heat sink and competes against the Joule heating, resulting in a net temperature decrease below the ambient. In the latter case, the Peltier effect acts as a heat source and reinforces the Joule heat, causing a sharp increase in temperature. In order to bring into sharper focus the influence of the Peltier effect, these curves can be compared with the dotted curve drawn for $\bar{\alpha} = 0$ and $\bar{J} = \overset{+}{-}\ 0.618$ (since the Seebeck coefficient is set to zero, the only remaining heat source is the Joule effect, which is independent of the direction of $\bar{J}$). The magnitude of the temperature differential between the dotted curve and the upper solid curve at any $\bar{t}$ is much larger than that for the lower one.

The length of the SMA, $\bar{d}$, is expected to have an influence on the extent of its cooling or

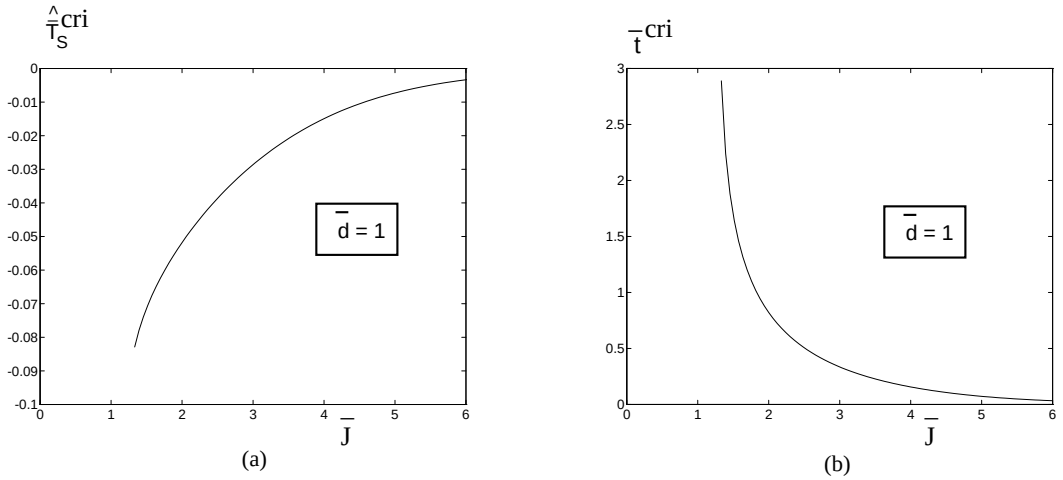

Figure 6: Dependence of the (a) critical value of the temperature, $\hat{\bar{T}}_s^{cri}$, and (b) critical value of time, $\bar{t}^{cri}$, on the current, $\bar{J}$.

heating. The average temperature, $\hat{\bar{T}}_S$, of the SMA has been presented as a function of the time $\bar{t}$ in Fig.5(a), at two values of $\bar{d}$, and two values of the current, $\bar{J} = 0.618$ and -0.618, shown as solid curves and dash-dot curves, respectively. As expected, a smaller $\bar{d}$ (or thinner SMA) is seen to result in a higher temperature change over a given length of time.

The magnitude of the current density, $\bar{J}$, also has a noticeable influence on the cooling or heating of the SMA. We examine such an influence in Fig.5(b). The solid curves correspond to increasing values of $\bar{J}$ (or increasing current density, J) resulting in increasing cooling. This indicates that the Peltier effect predominates. However, for $\bar{J} = 1.545$ (or $J = 5\ Amps/mm^2$ for the considered material properties and $d_p = 2mm$) corresponding to the dashed curve, though the cooling is comparatively higher and faster initially, the temperature, however, subsequently increases with time. A possible reason for such an occurrence (not a conclusive proof) is that if the current density increases beyond a certain value, the Joule heating causes significant distortion in the temperature profile; as a result, heat flows back into the SMA ($\vec{Q}_s.\hat{n} < 0$ for $\vec{J}.\hat{n} > 0$) rather than out of it. Hence, a $\hat{\bar{T}}_S - \bar{t}$ curve could have a turning point if $\bar{J}$ is high enough, marked by the point $(\hat{\bar{T}}_S^{cri}, \bar{t}^{cri})$ on the dashed curve. When the current direction is reversed ($\bar{J} < 0$), the Peltier effect now reinforces the Joule heating and no such turning point is observed, as is apparent from the monotonically increasing dash-dot curves in Fig.5(b). It is of interest to see how the critical point $(\hat{\bar{T}}_S^{cri}, \bar{t}^{cri})$ depends on $\bar{J}$. Such a critical point is located by numerically finding the value of $\hat{\bar{T}}_S$ and $\bar{t}$ for which $\frac{d\hat{\bar{T}}_S}{d\bar{t}} = 0$. We plot in Figs.6(a) and (b) the dependence of $\hat{\bar{T}}_S^{cri}$ and $\bar{t}^{cri}$, respectively, on $\bar{J}$, up to $\bar{J} \approx 6$ (corresponding to $J = 19.35\ Amps/mm^2$); only those points are plotted for which the critical time, $\bar{t}^{cri}$, is less than an arbitrarily chosen $\bar{t}^{cri} = 3$ (corresponding to $t = 32s$, in this case). It is interesting to see from Fig.6(a) that while the *magnitude* of $\hat{\bar{T}}_S^{cri}$ decreases monotonically with increasing $\bar{J}$ (due to the increasing dominance of the Joule effect over the Peltier effect), $\bar{t}^{cri}$ decreases too. This is especially relevant for the frequency of actuation; at high current densities, it is possible to cool the SMA very fast, although the extent of cooling decreases.

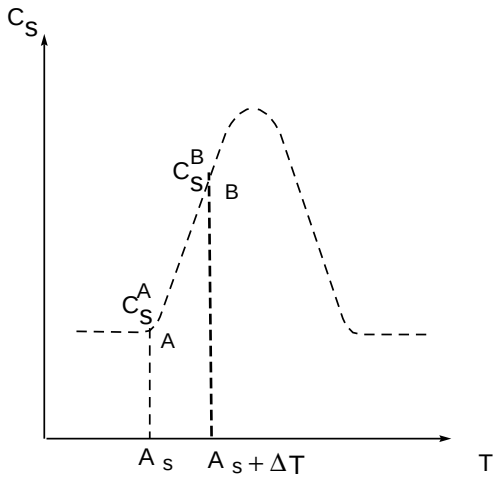

Figure 7: Schematic depiction of the changing heat capacity of the SMA during the phase transformation and its incorporation in the heat conduction problem.

4.2 Variable C_s (With phase transformation)

Till now, we have assumed that the heat capacity of the SMA remains constant. However, during a complete thermal cycle of heating and cooling, the SMA undergoes a phase transformation, with a change in its C_S, as given by Eqs.(7)-(8) and schematically depicted in Fig.3(a). Solution of such a problem incorporating a non-linear dependence in C_S is intractable, even in the 1-D case. Here, we approximately incorporate such a dependence by making a reasonable assumption that the C_S of the *entire SMA* is a function of its average temperature, computed from Eqs.(25) and (19), through Eqs.(7) and (8), for the forward and reverse transformations respectively.

The computational methodology to generate a complete thermal cycle will now be given. Starting from a fully *martensitic* SMA, the temperature profile of the SMA is computed from Eq.(19) for J < 0, with $\bar{T}_i^{in}(\bar{x}) = 0$ in Eq.(18) (i.e. the entire system starts from the ambient). When the average temperature of the SMA (computed from Eq.(25)) reaches A_s, the entire SMA is taken to be at the onset of the reverse transformation, M $\rightarrow$ A. The corresponding time, t (or $\bar{t}$), and the spatial temperature profile, $\bar{T}_i(\bar{x}, \bar{t})$, at that instant is recorded. Such a situation is depicted on the schematic curve in Fig.8 as the point A. The heat capacity at that point is marked as C_S^A. We now *intend* to march the solution ahead in time incrementally by Δt (yet unknown, or $\Delta\bar{t}$ being the increment in non-dimensional time) such that the average dimensional temperature in the SMA increases incrementally by ΔT to $A_s + \Delta T$, marked as the point B in Fig.7. At this temperature, the heat capacity is labeled as C_S^B. This amounts to discretizing the curve of $C_S - T$. We choose $\Delta T = 0.44^0 C$; the discretized curve appeared visually identical to the original, in Fig.7. It is the simple average of C_S^A and C_S^B which is used as the new heat capacity of the SMA to compute a new temperature profile by Eqs.(19) and (22) using $\bar{T}_i^{in}(\bar{x}) = \bar{T}_i(\bar{x}, \bar{t})$, where $\bar{T}_i(\bar{x}, \bar{t})$ was the normalized temperature profile at the onset of transformation (corresponding to point A in Fig.7 at normalized time $\bar{t}$). It is with this new value of C_S that we iteratively solve for the incremental time, Δt, at the end of which the average dimensional temperature in the SMA, $\hat{T}_s$, reaches $A_s + \Delta T$. The bisection method is chosen as the numerical scheme; the convergence criterion was based on an error defined by $\hat{T}_s - (A_s + \Delta T) \approx 1 \times 10^{-5}$. The entire process is then repeated over incremental

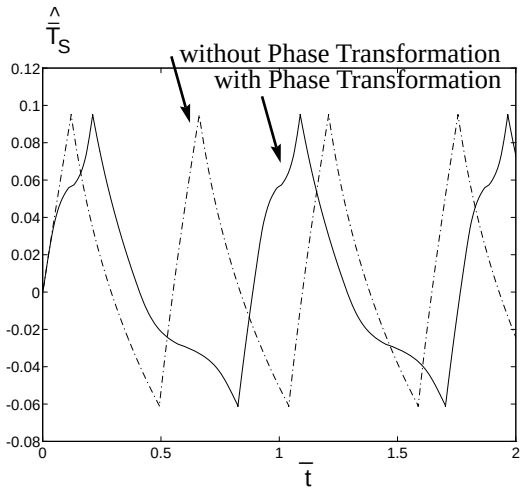

Figure 8: Comparison of the cyclic cooling curves of a SMA undergoing a phase transformation with one without a phase transformation.

changes in the average temperature (ensuring convergence at every step) until it reaches A_f and the transformation is fully completed. This process is further continued but now with a reversed value of J (J $>$ 0) to trigger the forward transformation.

For $\bar{J} = 0.618$ (or $J = 2Amps/mm^2$) the results of such a computation are shown in Fig.8 for a SMA undergoing a phase transformation (solid curve) or without (dash-dot curve) a phase transformation. The period of one cycle almost doubles due to the latent heat exchange accompanying the phase transformation and thus the change in the heat capacity is seen to contribute significantly to the time period for the thermal cycling.

The period of thermal cycling is dependent upon the volume fraction of the new phase that is formed. The cyclic curves in Fig.8 correspond to the situation in which the entire material is assumed to transform during the forward and reverse transformations. Starting from a fully martensitic SMA, the volume fraction of the martensite during the reverse transformation can be found from Eq.(11). The reverse transformation can be halted at a temperature below A_f, at which the untransformed martensite can be found from Eq.(11), and is denoted as ξ_M; the austenite formed will have a volume fraction $1 - \xi_M$. During the forward transformation, it is this volume fraction of austenite which undergoes the phase change to martensite. Thus instead of using C_s from Eq.(7) directly in the thermoelectric problem, a weighted value,$\xi_M C_s^0 + (1 - \xi_M)C_s$, is now used, during the forward transformation.

We display the change in volume fraction of martensite for $\xi_M = 0.25$, 0.5 and 1 and the associated cyclic temperature profile in Fig.9. The first case of 25% partial transformation is shown as a solid curve whereas the latter two cases corresponding to 50% and 100 % transformation are shown as dash-dot curves. It is seen that the time period of one cycle for full transformation, ranging from A to B in Fig.9(a), reduces by 50% for the partial transformation to $\xi_M = 0.5$ and by about 70 % for a partial transformation to $\xi_M = 0.25$. The thermal cycling consequently accelerates as it occurs within a shorter temperature range, as is evident from Fig.9(b).

It is evident that a higher frequency of actuation can be obtained only for a thinner SMA, at a high current density and with partial transformation. In order to get a feel for the dimensional

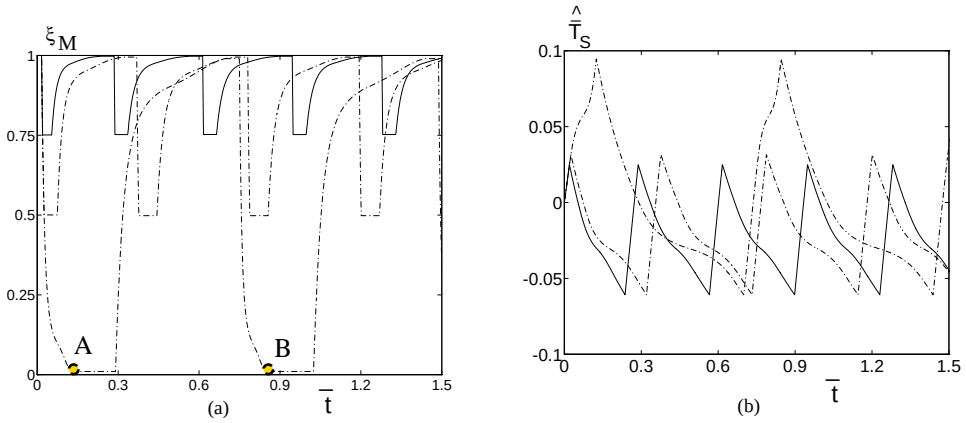

Figure 9: (a) Change in volume fraction of martensite and (b) cyclic temperature profile of SMA with partial and full transformation.

(rather than dimensionless) quantities involved, we plot the temperature T(0,t) versus time t in Fig.10 for a SMA with thickness $d_s = 0.5\ mm$, and at a (easy to realize) current density $J = 2.5\ Amps/mm^2$. It is seen that with full transformation the frequency is around 2 Hz, which increases to approximately 17 Hz when only a partial transformation of 25% is allowed.

Before concluding the parameteric study, it would be worthwhile to compare thermoelectric cooling with commonly used cooling mechanisms of natural and forced convection. We assume that a plate of SMA with thickness, $d_S = 1$ mm, commencing with a uniform temperature of 100^0C, is being cooled by three different methods: (a) thermoelectric cooling, (b) natural convection with h = 25 $\times 10^{-6}\ W/(mm^2 - K)$ and (c) forced convection with h = 200 $\times 10^{-6}\ W/(mm^2 - K)$ (Incropera and DeWitt, 1984). We make explicit the boundary and initial conditions for all three cases. With regard to the former (and referring Fig.2), we assume that at $t = 0$, the entire setup is at the ambient temperature, $T_0 = 25^0C$, except the SMA which is at 100^0C. For the purpose of this comparison that the "exposed" edges of N/SMA/P are insulated, thus setting $\bar{h} = 0$ in Eq.(1). The evolution of the temperature at a current density of $J = -0.625 Amps/mm^2$ is shown in Fig.11. The second case involves removing the N and P elements from the SMA and letting it cool from an initial temperature of 100^0C. As before, $h = 0$ on the thin edge of the SMA, but we allow convection on the two surfaces of the SMA originally in contact with the N and P. Thus, the 1-D formulation for this problem is described by Eq.(1), only for the SMA, with $J = 0, h_s = 0$. At $x = \overset{+}{-} \frac{1}{2} d_s$, $|\vec{Q}_s.\vec{n}| = h_p(T_S(x,t) - T_0)$. For cooling with natural convection, we use $h_p = 25 \times 10^{-6}$ W/(mm^2-K) and that with forced convection, we have $h_p = 200 \times 10^{-6} W/(mm^2 - K)$ (Incropera and DeWitt, 1984). It is seen from Fig.11 that thermoelectric cooling is relatively faster and reaches a temperature low enough to ensure a phase change.

5. EXPERIMENTAL RESULTS AND COMPARISON WITH THEORY

In order to verify the theoretical model for the thermoelectric cooling and heating described in the previous sections, experiments were conducted using a commercially available semiconductor material, namely, Bismuth-Telluride (P or N). The thermal load consisted of a rod of square cross-section made of either copper or Nitinol.

Figure 10: The predicted cyclic temperature-time plot of the SMA for full and partial transformation to 25%. The parameters used are: J = 2.5 $Amps/mm^2$, d_s = 0.5 mm, $d_p = d_n$ = 2 mm, $\alpha_p = -\alpha_n = 2.12 \times 10^{-4} V/K$.

Figure 11: Comparison of thermoelectric cooling with natural and forced convection.

Figure 12: Schematic of the Experimental Setup

The schematic of the experimental setup is depicted in Fig.12. The DC power supply consists of a current source. The purpose of the current reversal switch is to achieve both cooling and heating using the same power supply. The temperature measurement system, consisting of a thermocouple, an amplifier, a digital oscilloscope and a personal computer, is used to record the transient thermal response of the thermoelectric element.

In our studies, the commercially available semiconductor elements (P and N) used have a square cross section of 4 $\times$ 4 mm and a length of 2.12 mm. The thermal load has the same cross section as the semiconductors, with the length being 6.22 mm for copper and 5.41 mm and 1.19 mm respectively, for the two samples of Nitinol. In order to simulate isothermal boundary conditions, we used two big blocks of aluminium as the heat sinks. For calibration purposes, the temperature of the heat sinks was also measured using thermocouples, and was found to remain constant to within 1^0 C throughout the experiment. In our theoretical model, it was assumed that the interfaces are thermally perfect. In other words, there is no contact resistance which causes heating at the interfaces between the thermal load and the semiconductors. Therefore, for a reasonable comparison it is important to minimize such heating effects in our experiments. In the case of copper, the interfaces do not present a problem since they were tin-soldered. However, in the case of Nitinol, it was found impossible to tin-solder Nitinol to bismuth-telluride. Therefore, we simply cleaned the surfaces using acetone and assembled the element with only a mechanical coupling between the interfaces. The cooling element is sandwiched between the heat sinks which are held together by the pressure applied using a C clamp.

For the transient temperature measurement system, a fast response thermocouple (with a typical response time of 2- 5 ms) together wih an amplifier (with a response frequency of greater than 100 Hz, a gain setting of 100, and an automatic cold-junction compensation) is used. The output from the amplifier is fed into a Tektronix digital oscilloscope. The error of this transient temperature measurement, when properly calibrated with boiling water, is estimated to be 1 K.

A silicon paste which has high thermal conductivity, but low electrical conductivity, is used to

Figure 13: Comparison of the heating and cooling curves between experiment and prediction, for Copper, with $|J| = 0.655\ Amps/mm^2$.

connect the thermocouple and the thermal load. Due to the high thermal conductivity of copper and SMA materials, it is reasonable to assume that the temperature is uniform across the cross-section. At time t=0, a constant current is applied to the cooling element. The digital oscilloscope is synchronously triggered at time t=0. The position of the double-throw switch is determined by whether cooling or heating is desired. Typically, the length of the temperature measurment record is 1024 points with a total recording time of about 50 seconds. The measured and predicted transient responses of a copper thermal load are compared in Fig.13. The Seebeck coefficient of copper, $\alpha_{cu} = 1.3 \times 10^{-6} V/K$ (Mac Donald, 1962), and thus $\alpha_p = 165\alpha_{cu}$. In the analytical model, the Seebeck coefficient of copper is taken as zero. The conductivity, resistivity and heat capacity of copper are taken as $0.401\ W/(mm-K)$, $1.678 \times 10^{-5}\ \Omega - mm$ and $3.462 \times 10^{-3}\ J/mm^3$ respectively (Aesar, 1992). The agreement is far better during cooling than it is during heating. At this time, we have no satisfactory explanation for this observation; we offer a plausible conjecture. In our current model we have assumed that the various material properties are independent of temperature over the range of temperature encountered in our experiments. Suppose, however, that there is some temperature dependence. We now observe that the temperature excursion during heating ($\approx 60^0 C$) is significantly larger than that during cooling ($\approx 30^0 C$). This (conjectured) source of error will affect the heating curve more than the cooling curve. In order to test this conjecture, we are in the process of modifying the model to include this effect. The next two figures (Figs.14 and 15) show the thermal response of SMA specimens of thickness 5.41 mm and 1.19 mm respectively. These are heated (cooled) from martensite to austenite (austenite to martensite). The former is endothermic in nature whereas the latter is exothermic, both represented by an increase in the heat capacity, C_s, from its original value, C_s^0, in absence of phase transformation. For a given heat input(or output) rate into(or from) the SMA, a higher heat capacity implies a lower rate of temperature change. As the phase transformation is completed, the heat capacity is restored to its original lower value, C_s^0. It is thus expected that the high rate of temperature change will be restored after completion of

Figure 14: Comparison of the heating and cooling curves between experiment and prediction, for SMA with thickness, $d_s = 5.41$ mm and $|J| = 0.625\ Amps/mm^2$.

Figure 15: Comparison of the heating and cooling curves between experiment and prediction, for SMA with thickness, $d_s = 1.19$ mm and $|J| = 0.625\ Amps/mm^2$.

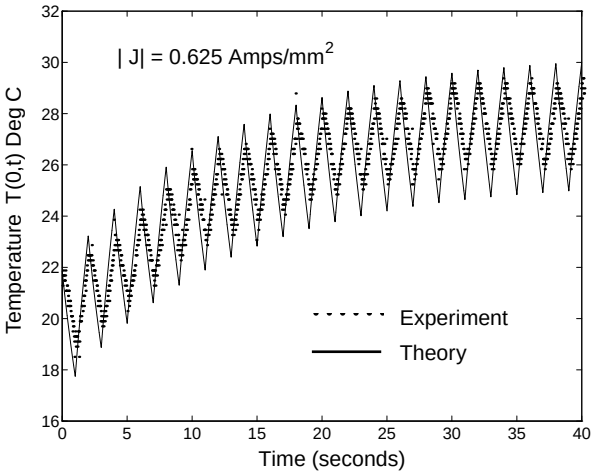

Figure 16: Comparison of the cyclic thermal response between experiment and prediction, for copper with thickness, $d_s = 4$ mm.

the phase transformation. This is manifested in the distortions of the heating and cooling curves in Figs.14 and 15, resulting in a delay in the heating and cooling times.

Finally, we turn to Fig.16 for a comparison of the cyclic thermal response of the experiment(shown with a dotted line) and the theory(shown with a continuous line) for copper. The magnitude of the current density is kept at $|J| = 0.625 Amps/mm^2$. Starting at an ambient temperature of 296 K, the copper is first cooled for 1 sec.(with the current direction from the N to the P for cooling) and heated for 1 sec.(with the current direction now reversed). This process is repeated in time with a frequency of 0.5 Hz. Notice that the temperature range of each cycle gradually increases in time, as reflected by the upward trend of the curve. As we allow equal times for heating and cooling in each cycle, the heating will dominate since it is faster than the cooling, resulting in a upward shift of the temperature range. In order to maintain the same temperature range for each cycle, the time allowed for cooling in each cycle has to be higher than that of the heating, a process that we are currently implementing in our laboratory. However, the cyclic curve displayed is nonetheless useful in comparing the theory and experiment; the comparison is reasonable. Note that the frequency of 0.5 Hz can be boosted by increasing the current density or/and reducing the thickness of the SMA(the value of d_s).

CONCLUSIONS

As a first step towards developing a large force and large strain actuator using a thermoelectric heat exchange mechanism, we have developed a simple 1-D analytical model to model the thermoelectric heat transfer problem. The solution is capable of taking into account numerically the change in the heat capacity of a SMA undergoing phase transformation. Experiments have been implemented in the laboratory and comparison with the theory validates the use of the 1-D model. It has been theoretically demonstrated that when $d_s = 0.5$ mm , $d_p = 2$ mm and $|J| = 2.5 Amps/mm^2$, and the SMA is taken through one complete cycle of heating and cooling, a frequency of 2 Hz is obtained on full transformation. The frequency under the same conditions can be enhanced to

about 17 Hz if only 25% of phase transformation is allowed. With the existing experimental setup where $d_s = 4$mm, $d_p = 2.12$mm and $|J| = 0.625 Amps/mm^2$, it has been possible to demonstrate a frequency of 0.5 Hz for copper. We are currently working not only to enhance the frequency of this thermal cycling but also to model and design the thermomechanical response of the actuator.

ACKNOWLEDGEMENT

This work was supported by the Grant No. N 00014-94-1-0268 from the Office of Naval Research to Texas A&M University, College Station. The continuing interest by Dr. Roshdy Barsoum in the evolution of this work is gratefully acknowledged.

REFERENCES

1. "Aesar", John Matthey Co., 1992.

2. Bo, Z. and Lagoudas, D.C., 1994, "Deformations and Thermal Response of Active Flexible Rods with Embedded SMA Actuators", Smart Structures and Materials 1994: Smart Structures and Intelligent Systems, Proceedings of the SPIE 1994 North American Conference on Smart Structures, Orlando, FA, Feb 13-18, 1994, Vol. 2190.

3. Boyd, J.G., and Lagoudas, D.C., 1994, "Thermomechanical Response of Shape Memory Composites", *Journal of Intelligent Materials and Structures*, Vol. 5, pp. 333-346.

4. Buckingham, E., 1914, "On Physically Similar System Illustrations of the Use of Dynamical Equations", Phys. Rev., Vol. 4, pp. 345-376.

5. deBlonk, B.J., 1995, "Fabrication and Evaluation of SMA-Silicone Rubber Continuous-Fiber and Particulate Composites",*M.S. Thesis*, Texas A&M University.

6. Domenciali, C.A., 1954, "Irreversible Thermodynamics of Thermoelectricity", *Reviews of Modern Physics*, Vol. 26, No.2 , pp. 237-275.

7. Harman, T.C., and Honig, J.M., 1967, "Thermoelectric and Thermomagnetic Effects and Applications", Mc-Graw Hill Book Co., New York.

8. Incropera, F.P., and DeWitt, D.P., "Introduction to Heat Transfer", John Wiley and Sons, NY, 1984.

9. Jackson, C.M., Wagner, H.J., and Wasilewski, 1972, "A report on 55-Nitinol – The Alloy with a Memory: Its Physical Metallurgy, Properties and Applications", Technology Untilization Office, NASA, Washington, D.C..

10. Lagoudas, D.C. and Kinra, V.K., 1993, "Design of High Frequency SMA Actuators, Disclosure of Invention TAMUS 803, Texas A&M University, College Station, TX 77843.

11. Liang, C. and Rogers, C.A., 1990, "One-Dimensional Thermomechanical Constitutive Relations for Shape Memory Materials", Proceedings, *AIAA 32nd Structures, Structural Dynamics and Materials Conference*, baltimore, MD.

12. MacDonald, D.K.C., "Thermoelectricity: An Introduction to the Principles", John Wiley and Sons, NY, 1962.

13. Melcor Educational Package, MELCOR, TRENTON, NJ, USA, 1992.

14. Takagi, T., 1990, "A Concept of Intelligent Materials", *Journal of Intell. Mater. Sys. and Struct.*, Vol.1, pp.149-156.

15. Tanaka, K., 1986, "A Thermomechanical Sketch of Shape Memory Effect: One-Dimensional Tensile Behavior", *Res Mechanica*, Vol. 18, pp. 251-263.

16. Thrasher, M.A., Shahin, A.R., Meckl, P.H., and Jones, J.D., 1992, "Thermal Cycling of Shape Memory Alloy Wires using Semiconductor Heat Pump Modules", *Proceedings of the 1st European Conference on Smart Structures and Materials*, Glasgow, England.

17. Tittle, C.W., 1965, "Boundary Value Problems in Composite Media: Quasi-Orthogonal Functions", *Journal of Applied Physics*, vol. 36, pp. 1486-1488.

18. Wada, B.K., Fanson, J.L. and Crawley, E.F., 1990, "Adaptive Structures", *Journal of Intell. Mater. Sys. and Struct.*, Vol.1, pp.157-174.

APPENDIX

The parameters C_1, C_2 and B_n used in Eqs. (20),(21),(23) and (24) follow as

$$C_1 = UC_2 + V \ , \quad \text{and} \quad C_2 = \frac{\bar{J}^2\bar{h}^{-1}\bar{k}^{-1}\left(1-e^{\sqrt{\bar{h}}}\right) - \bar{\rho}\bar{J}^2\bar{h}^{-1}\bar{k}^{-1} - 2Vcosh\left(\sqrt{\bar{h}\bar{k}^{-1}}\bar{d}\right)}{2Ucosh\left(\sqrt{\bar{h}\bar{k}^{-1}}\bar{d}\right) + e^{\sqrt{\bar{h}}(\bar{d}+2)} - e^{\sqrt{\bar{h}\bar{k}^{-1}}\bar{d}}} \ . \quad (26)$$

The parameters U and V are

$$U = \frac{\sqrt{\bar{h}}\bar{k}^{-1}\left[e^{\sqrt{\bar{h}}\bar{d}} + e^{\sqrt{\bar{h}}(\bar{d}+2)}\right]}{2\left[\sqrt{\bar{h}\bar{k}^{-1}}sinh\left(\sqrt{\bar{h}\bar{k}^{-1}}\bar{d}\right) + \bar{\alpha}\bar{J}\bar{k}^{-1}cosh\left(\sqrt{\bar{h}\bar{k}^{-1}}\bar{d}\right)\right]} \ , \quad (27)$$

and

$$V = \frac{\frac{\bar{J}^2}{\sqrt{\bar{h}}\bar{k}}.e^{\sqrt{h}} - \bar{\alpha}\bar{J}\bar{k}^{-1}\left(1+\frac{\bar{\rho}\bar{J}^2}{\bar{h}}\right)}{2\left[\sqrt{\bar{h}\bar{k}^{-1}}sinh\left(\sqrt{\bar{h}}\bar{d}\right) + \bar{\alpha}\bar{J}\bar{k}^{-1}cosh\left(\sqrt{\bar{h}}\bar{d}\right)\right]} \ . \quad (28)$$

The coefficients, B_n, remain to be given. These are

$$B_n = D_n^{-1}.\left\{-\bar{C}\int_0^{\bar{d}}\left(\bar{T}_s^{in}(|\bar{x}|) - \bar{T}_s^{s}(|\bar{x}|)\right).\frac{sin\beta_{p,n}cos(\beta_{s,n}|\bar{x}|)}{cos\left(\beta_{s,n}\bar{d}\right)cos\left(\beta_{p,n}\left[1+\bar{d}\right]\right)}d|\bar{x}|\right.$$
$$\left. + \int_{\bar{d}}^{1+\bar{d}}\frac{\left(\bar{T}_P^{in}(|\bar{x}|) - \bar{T}_P^{s}(|\bar{x}|)\right).sin\beta_{p,n}(|\bar{x}|-1-\bar{d})}{cos\left(\beta_{p,n}\left[1+\bar{d}\right]\right)}d|\bar{x}|\right\} \quad (29)$$

with

$$2D_n = \bar{C}\frac{sin^2\beta_{p,n}}{cos^2\left(\beta_{s,n}\bar{d}\right)cos^2\left(\beta_{p,n}\left[1+\bar{d}\right]\right)}\left[\bar{d} + \frac{1}{2\beta_{s,n}}sin\left(\beta_{s,n}\bar{d}\right)\right]$$
$$+cos^2\left(\beta_{p,n}\left[1+\bar{d}\right]\right)\left[1 - \frac{sin2\beta_{p,n}}{\beta_{p,n}}\right] \ , \quad (30)$$

where the nth eigenvalue corresponding to the ith phase, $\beta_{i,n}$ follows from the solution of the following equations

$$\bar{K}\beta_{s,n}tan\left(\beta_{s,n}\bar{d}\right) = \beta_{p,n}cot\beta_{p,n} + \bar{\alpha}\bar{J} \ ,$$
$$\beta_{p,n} = \sqrt{\frac{\bar{K}}{\bar{C}}\beta_{s,n}^2 + \bar{h}\left(\frac{1}{\bar{C}} - 1\right)} \ . \quad (31)$$